

# Optimal Pulse Width Modulation of Three-Level Converters With Reduced Common-Mode Voltage

Isavella Koukoula, *Student Member, IEEE*, Petros Karamanakos, *Senior Member, IEEE*,  
and Tobias Geyer, *Fellow, IEEE*

**Abstract**—This paper presents the computation of three-level optimized pulse patterns (OPPs) that limit the common-mode voltage (CMV) and generate currents with low harmonic distortions. This is achieved by relaxing the symmetry properties of conventional OPPs and by reformulating the associated optimization problem accordingly. As demonstrated by the presented numerical results for a three-level converter driving a medium-voltage (MV) induction machine, the computed OPPs not only limit the CMV but also produce very low harmonic distortions, in some cases even lower than those of conventional OPPs. Experimental results based on a scaled-down, low-voltage (LV) drive system serve as a proof of concept, highlighting the benefits of the proposed OPPs.

**Index Terms**—Optimized pulse patterns (OPPs), three-level converters, synchronous optimal pulse width modulation, quarter-wave symmetry, half-wave symmetry, medium-voltage (MV) drives.

## I. INTRODUCTION

THREE-level converters, such as the neutral-point-clamped (NPC) converter, are widely used in high-power electronics applications [1]. Their switched three-phase output voltage is typically generated by means of pulse width modulation (PWM). Intrinsicly, this voltage has a common-mode (CM) component that has adverse effects on the load. In drive systems, e.g., the common-mode voltage (CMV) is the main cause of parasitic bearing currents, which can damage the bearings [2]. The CMV also increases the stress on the motor insulation. In transformer-less photovoltaic (PV) converter-based systems, the CMV leads to leakage currents that can deteriorate the system performance while posing potential safety risks [3], [4]. Hence, PWM methods that can effectively limit the CMV are advantageous.

Different PWM techniques that achieve *complete* elimination of the CMV were proposed in [5]. These techniques utilize only the voltage vectors that produce zero CMV. In all these modulation techniques the linear modulation range is limited to 1 (out of  $4/\pi$ ). Additionally, the harmonic distortions and switching events per modulation cycle are increased, leading to an increase in power losses. Furthermore, the short voltage vectors are not used, meaning there are no redundant states that could be used for balancing the neutral point potential of

an NPC converter. Finally, as simultaneous switching in two phases is required for zero CMV, elaborate techniques for the deadtime compensation are required [6], [7].

For these reasons, *partial* elimination of the CMV is a good compromise between a low CMV and less adverse effects on the harmonics and dc-link voltage utilization. To this aim, carrier-based PWM (CB-PWM) with phase-opposite disposition (POD-PWM) was proposed for three- and five-level converters in [8] and [9], respectively. By limiting the CMV, however, this PWM method significantly increases the total demand distortion (TDD) of the current compared with CB-PWM. Moreover, as this method allows two phases to switch simultaneously the switching devices may be damaged. This pitfall, nevertheless, can be addressed by modifying the carriers of the three-level PWM as shown in [10]. Furthermore, to improve the current TDD while still limiting the CMV, modified space vector modulation (SVM) methods can be employed [11]. Such methods imitate two-level SVM while selecting only these voltage vectors that keep the CMV low. This principle, however, leads to the underutilization of the dc-link voltage as the maximum achievable modulation index—similar to CB-PWM methods—is limited to 1 (out of  $4/\pi$ ). The SVM methods proposed in [12] and [13], however, tackled this issue, and thus reached the maximum modulation index that can be achieved with SVM, i.e.,  $2/\sqrt{3}$ , by adopting different voltage-vector sequences. In doing so, however, the harmonic distortions either significantly increase [12], or more switching commutations per modulation cycle are required when comparing with conventional SVM, thus resulting in higher switching losses [13]. Additionally, there are discontinuous space vector-based PWM strategies that manage to limit the CMV [14]. However, this feature is achieved only for a limited range of modulation indices, while the inherent disadvantages of SVM techniques, such as the limited utilization of the dc-link voltage and poor harmonic performance at very low switching frequencies, are also present.

As an alternative to CB-PWM and SVM, programmed PWM methods, such as selective harmonic elimination (SHE) [15] and optimized pulse patterns (OPPs) [16], can be considered as they can produce lower harmonic distortions. Regarding SHE, the switching angles (i.e., switching time instants) of the switching pattern are computed in an offline procedure by solving a system of nonlinear equations that aims to eliminate specific harmonics. As the to-be-eliminated harmonics can be freely chosen, the SHE problem can be formulated such that the CMV is limited. As shown in [17], this can be achieved by eliminating the low-order triplen

The work of I. Koukoula was supported by ABB Oy Drives. The work of P. Karamanakos was supported by the Research Council of Finland.

I. Koukoula and P. Karamanakos are with the Faculty of Information Technology and Communication Sciences, Tampere University, 33101 Tampere, Finland; e-mail: isavella.koukoula@tuni.fi, p.karamanakos@ieee.org

T. Geyer is with ABB System Drives, 5300 Turgi, Switzerland; e-mail: t.geyer@ieee.org

harmonics. The absence of CM harmonics, however, limits the range of operation, as the maximum achievable modulation index is 1. The SHE method in [18] manages to partially eliminate the CMV while expanding the modulation index range from  $[0, 1]$  to  $[0, 2/\sqrt{3}]$  by means of optimal third-harmonic injection at high modulation indices. A derivative of SHE, namely hybrid selective harmonic mitigation (SHM), that achieves CMV reduction was proposed in [19]. By eliminating the low-order triplen harmonics and mitigating the low-order non-triplen harmonics the rms of the CMV is reduced, while the current TDD is improved compared with that of SHE with limited CMV. Nevertheless, similarly to [17], since the low-order CM harmonics are eliminated the dc-link voltage is not fully utilized as a modulation index greater than 1 cannot be achieved.

As for the OPPs, these are a PWM method that produces the lowest possible harmonic distortions [16]. The optimal PWM patterns (in terms of switching angles and switch positions) are computed in an offline procedure by minimizing an objective function that accounts for the TDD of the load current. In doing so, the harmonic motor losses and the peak current are also reduced [20]. Hence, OPPs are a very good candidate for limiting the CMV while still producing currents of high quality.

In this direction, and when considering three-level OPPs, only a few works have been presented that compute OPPs with limited CMV, see e.g., [21] and [22]. In [21], *complete* elimination of the CMV was proposed. As with other PWM methods, this is achieved at the cost of underutilization of the dc-link voltage as the modulation index is limited to  $2\sqrt{3}/\pi$ , while at least two phases have to switch simultaneously. On the contrary, [22] aims to keep the CMV below a desired (nonzero) value. To do so, the *finite* sum of CM harmonics is kept bounded. However, since this sum merely approximates the CMV (instead of providing its exact value), and the upper bound on the CMV is heuristically chosen, suboptimal OPPs may be computed.

In both of the aforementioned works the benefits of OPPs are not fully exploited as the limitation of the CMV occurs at the expense of increased harmonic distortions. To mitigate this issue, this work reformulates the OPP optimization problem by dropping artificial restrictions of the conventional OPP problem. Specifically, as presented in [23], relaxing the symmetry properties of the OPPs with limited CMV increases the search space of the optimization problem, and as a result, a deterioration in the current quality can be avoided. The resulting OPPs have current TDDs that are very close to—if not lower than—those of the conventional unconstrained OPPs, while keeping the CMV limited over the *whole* range of modulation indices, i.e., while fully utilizing the available dc-link voltage. This paper extends this work by providing more insight into the features of the proposed OPPs acquired based on a medium-voltage (MV) drive consisting of a three-level inverter and an induction machine. To this end, more numerical results are provided and discussed. Moreover, to better highlight the advantages of the proposed optimal modulation method, it is compared with other methods that limit the CMV. Finally, to assess their effectiveness in a real-world setting, the computed

OPP are applied to a scaled-down, low-voltage (LV) drive system.

This paper is structured as follows. Section II presents the CMV along with the strategy adopted to limit it. Subsequently, the relevant OPP optimization problem is derived. In Section III, the associated numerical results are presented and discussed in detail. Section IV offers a comparison with CB-PWM methods that reduce the CMV in terms of current TDD. Moreover, the real-world performance verification of the computed OPPs in a LV drive setup is presented in Section V. Finally, Section VI concludes this paper.

## II. OPPS WITH REDUCED COMMON-MODE VOLTAGE

Assume a three-level converter and let  $\theta$  denote the angle of the pulse pattern. The pulse number  $d$  is defined as the ratio between the device switching frequency  $f_{sw}$  and the fundamental frequency  $f_1$ , i.e.,  $d = \frac{f_{sw}}{f_1}$ . With the above, a  $2\pi$  (i.e., full-wave) periodic switching waveform  $u(\theta)$  is fully described by  $4d + 1$  switch positions  $u_i \in \{1, 0, -1\}$  with  $i \in \{0, \dots, 4d\}$ , and  $4d$  primary switching angles  $\alpha_i, i \in \{1, \dots, 4d\}$ . At each switching angle  $\alpha_i$  a switching transition  $\Delta u_i = u_i - u_{i-1} \in \{1, -1\}$  occurs. Note that due to the  $2\pi$ -periodicity, the initial and the last switch positions are the same, i.e.,  $u_0 = u_{4d}$ .

### A. Objective Function

OPP are computed by minimizing an objective function that captures the load current TDD. Assuming an inductive load, the current TDD is given by

$$I_{\text{TDD}} = \frac{1}{\underbrace{\sqrt{2}I_{\text{nom}}\omega_1 X}_{\text{constant}}} \frac{V_{\text{dc}}}{2} \sqrt{\sum_{n \neq 1} \left(\frac{\hat{u}_n}{n}\right)^2} = c\sqrt{J}. \quad (1)$$

The term  $c$  depends only on the converter and load parameters, namely, the nominal current  $I_{\text{nom}}$ , the fundamental angular frequency  $\omega_1$ , the load reactance  $X$ , and the dc-link voltage  $V_{\text{dc}}$ . Hence,  $c$  can be considered a (constant) scaling factor. Thus, it can be discarded as it does not affect the optimization result. In doing so, the objective function  $J$  of the OPP problem accounts only for the (weighted) harmonics of the pulse pattern. The amplitude of the  $n^{\text{th}}$  harmonic is given by  $\hat{u}_n = \sqrt{a_n^2 + b_n^2}$ , with  $a_n$  and  $b_n$  being the Fourier coefficients of the periodic OPP waveform. For the analytical expressions of the Fourier coefficients, the reader is referred to [24].

### B. Conventional OPP Problem

Conventional OPPs have the following properties: (P1) three-phase symmetry, i.e., if the OPP for phase  $a$  is  $u_a(\theta) = u(\theta)$ , then  $u_b(\theta) = u(\theta - \frac{2\pi}{3})$  and  $u_c(\theta) = u(\theta + \frac{2\pi}{3})$  are the OPPs for phases  $b$  and  $c$ , respectively; (P2) half-wave symmetry, i.e.,  $u(\theta) = -u(\theta + \pi) \forall \theta \in [0, \pi]$ ; and (P3) quarter-wave symmetry, i.e.,  $u(\theta) = u(\pi - \theta) \forall \theta \in [0, \frac{\pi}{2}]$ . Moreover a fourth property (P4) relates to the switching sequence, namely unipolar switching is assumed while the first switch position is always zero, i.e.,  $u(\theta) \geq 0, \forall \theta \in [0, \frac{\pi}{2}]$ , and  $u_0 = 0$ . An OPP with these properties is shown in Fig. 1(a).

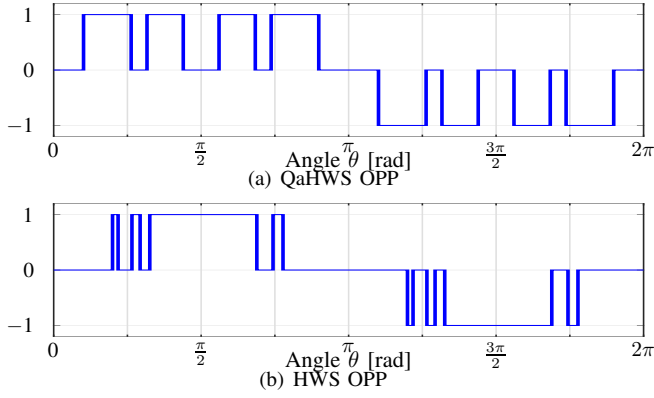


Fig. 1: Examples of OPPs with different symmetry properties for  $d = 4$  at modulation index  $m = 0.8$ .

The above properties imply that for the computation of conventional OPPs, hereafter referred to as quarter- and half-wave symmetric (QaHWS) OPPs, only the  $d$  switching angles  $\alpha_1, \dots, \alpha_d \in [0, \pi/2]$  of  $u_a$  are required to fully characterize the three-phase OPP. Hence, the corresponding optimization problem is of the form

$$\begin{aligned} & \underset{\alpha_Q}{\text{minimize}} && J_1(\alpha_Q) = \sum_{n=5,7,\dots} \left(\frac{b_n}{n}\right)^2 \\ & \text{subject to} && b_1 = m \\ & && 0 \leq \alpha_1 \leq \alpha_2 \leq \dots \leq \alpha_d \leq \frac{\pi}{2}, \end{aligned} \quad (2)$$

where  $\alpha_Q = [\alpha_1 \ \alpha_2 \ \dots \ \alpha_d]^T$ , and  $m \in [0, 4/\pi]$  is the desired modulation index. Note that due to the QaHWS, the  $a_n$  Fourier coefficients are zero. Moreover, triplen harmonics are not considered as they do not drive harmonic current when the star point of the load floats [24]. As a result, only the harmonics at non-triplen, odd multiples of the fundamental frequency are taken into account in (2).

### C. Common Mode

The CMV is defined as the average of the three single-phase output voltages of the inverter  $v_x$ , with  $x \in \{a, b, c\}$ , and it can assume values  $\pm zV_{dc}/6$ , with  $z = 0, 1, 2, 3$ , when three-level converters are considered. Since it holds that  $v_x = \frac{V_{dc}}{2}u_x$ , it directly follows that the *common-mode (CM) switch position*  $u_o$  is defined as

$$u_o(\theta) = \frac{u_a(\theta) + u_b(\theta) + u_c(\theta)}{3}, \quad (3)$$

with  $u_o = \pm z/3$ . The CM switch position  $u_o$  is a  $\frac{2\pi}{3}$ -periodic signal, and inherits the symmetry properties of the OPP.

Consider an OPP with half-wave symmetry (HWS). This implies that the CM switch position  $u_o$  exhibits HWS as well. As a result, the necessary information to compute  $u_o$  based on the three-phase OPP  $\mathbf{u}_{abc}(\vartheta) = [u_a(\vartheta) \ u_b(\vartheta) \ u_c(\vartheta)]^T$ , with  $\vartheta \in [0, \frac{\pi}{3}]$ , is included in the single-phase OPP  $u(\theta)$  for  $\theta \in [0, \pi]$  as the following hold:

- $u_a(\vartheta)$  is identical to the first  $\frac{\pi}{3}$ -segment of  $u(\theta)$ , see the blue segment in Fig. 2.
- $u_b(\vartheta)$  is identical to the second  $\frac{\pi}{3}$ -segment of  $-u(\theta)$ , see the red segment in Fig. 2. Therefore,  $u_b(\vartheta) = -u(\vartheta + \frac{\pi}{3})$ ,  $\vartheta \in [0, \frac{\pi}{3}]$ .

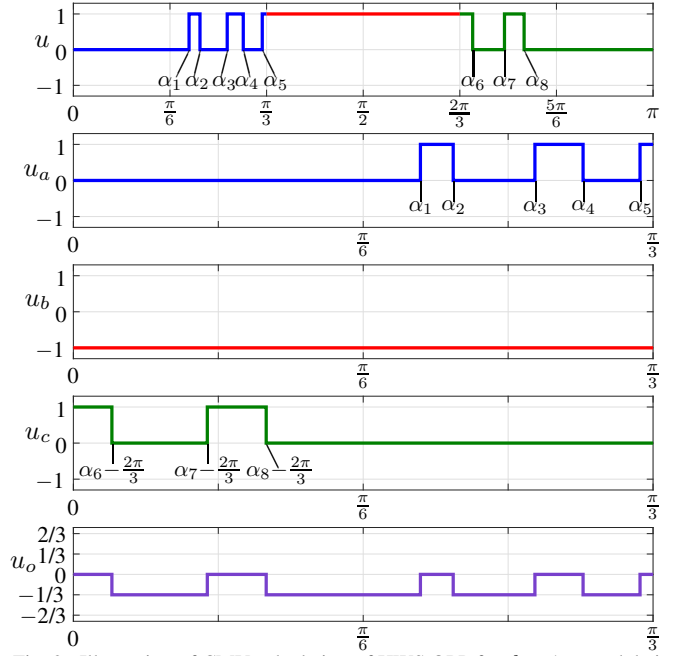


Fig. 2: Illustration of CMV calculation of HWS OPP for  $d = 4$  at modulation index  $m = 0.8$

- $u_c(\vartheta)$  is identical to the third  $\frac{\pi}{3}$ -segment of  $u(\theta)$ , see the green segment in Fig. 2. Hence  $u_c(\vartheta) = u(\vartheta + \frac{2\pi}{3})$ ,  $\vartheta \in [0, \frac{\pi}{3}]$ .

In a similar fashion, if the OPP is QaHWS then  $u_o$  exhibits QaHWS too, and  $u_o$  can be constructed based on the information included in the three-phase OPP  $\mathbf{u}_{abc}(\vartheta)$  for  $\vartheta \in [0, \frac{\pi}{6}]$ , which can be derived from the single-phase OPP  $u(\theta)$ ,  $\theta \in [0, \frac{\pi}{2}]$  as follows:

- $u_a(\vartheta)$  is identical to the first  $\frac{\pi}{6}$ -segment of  $u(\theta)$ , see the blue segment in Fig. 3.
- $u_b(\vartheta)$  is identical to the third  $\frac{\pi}{6}$ -segment of  $-u(\theta)$ , see the red segment in Fig. 3. This means that  $u_b(\vartheta) = -u(\vartheta + \frac{\pi}{3})$ ,  $\vartheta \in [0, \frac{\pi}{6}]$ .
- $u_c(\vartheta)$  is identical to the mirrored second  $\frac{\pi}{6}$ -segment of  $u(\theta)$ , see the green segment in Fig. 3. This means that  $u_c(\vartheta) = u(\frac{\pi}{3} - \vartheta)$ ,  $\vartheta \in [0, \frac{\pi}{6}]$ .

### D. Common-Mode Constraint

To reduce the bearing currents, the magnitude of the CMV, its rate of change  $dv_o/dt$  as well as the frequency of the changes in CMV must be low [25]. When three-level OPPs are applied to a converter the value of  $dv_o/dt$  is fixed to  $V_{dc}/6$ , assuming that two switches do not switch at the same time, while the CMV value changes  $4d$  times within the fundamental period of the CMV. This means that magnitude of the CMV is the only variable that can be manipulated, i.e., reduced. Since *complete* elimination of the CMV has the disadvantages of limited use of the available voltage and high harmonic distortions, we aim to limit the CMV to  $V_{dc}/6$ . Therefore, a constraint of the form

$$\max(|u_o(\theta)|) \leq \frac{1}{3}, \quad (4)$$

is added to the OPP optimization problem (2). For the implementation of (4), the maximum absolute value of  $u_o$  needs to

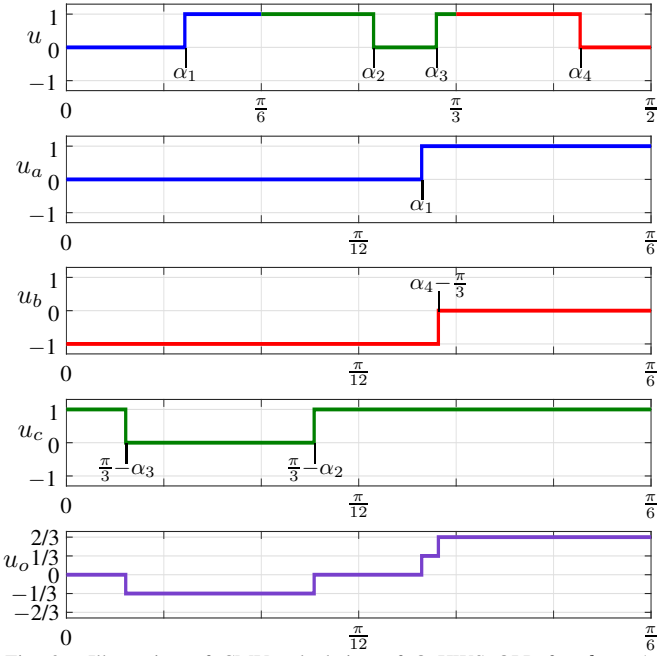


Fig. 3: Illustration of CMV calculation of QaHWS OPP for  $d = 4$  at modulation index  $m = 0.8$

### Algorithm 1 Constraint on common-mode switch position

For OPPs with QaHWS:

1. Given  $u(\theta)$ , with  $\theta \in [0, \frac{\pi}{2}]$ , construct the three-phase OPP  $\mathbf{u}_{abc}(\theta)$  for  $\theta \in [0, \frac{\pi}{6}]$ , based on symmetry properties (P1)–(P3).
  2. Sort the  $d$  switching angles of  $\mathbf{u}_{abc}$  in ascending order.
  3. Calculate  $u_o$  by cumulative summing up the corresponding switching transitions  $\Delta u(\alpha_i)$  for  $0 \leq \alpha_i \leq \frac{\pi}{6}$ .
- Return  $u_o(\theta)$  for  $\theta \in [0, \frac{\pi}{6}]$ .

For OPPs with HWS:

1. Given  $u(\theta)$ , with  $\theta \in [0, \pi]$ , construct the three-phase OPP  $\mathbf{u}_{abc}(\theta)$  for  $\theta \in [0, \frac{\pi}{3}]$ , based on symmetry properties (P1)–(P2).
  2. Sort the  $2d$  switching angles of  $\mathbf{u}_{abc}$  in ascending order.
  3. Calculate  $u_o$  by cumulative summing up the corresponding switching transitions  $\Delta u(\alpha_i)$  for  $0 \leq \alpha_i \leq \frac{\pi}{3}$ .
- Return  $u_o(\theta)$  for  $\theta \in [0, \frac{\pi}{3}]$ .

be calculated during the OPP computation process. To do so, the procedure described in Algorithm 1 is adopted. Nevertheless, the introduction of (4) compromises the current TDD, as a degree of freedom in the minimization of  $I_{TDD}$  is removed, as also demonstrated in the numerical results presented in Section III. To address this issue, the optimization problem that computes OPPs with constrained CMV is reformulated, as discussed in the following section.

### E. OPP Problem with Common-Mode Constraint

As recently shown in [24], relaxing the OPP properties increases the search space of the three-level OPP problem, and thus the degrees of freedom during the OPP computation process. Motivated by this, in this work, we relax the symmetry and switching properties. Namely, we drop properties (P3) and (P4). By dropping (P3), half-wave symmetric (HWS) OPPs result, meaning that  $2d$  switching angles need to be

computed, as opposed to the  $d$  angles computed for QaHWS OPPs. A HWS OPP is depicted in Fig. 1(b). Relaxing the unipolar switch positions and  $u_0 = 0$  (see property (P4)), i.e., allowing for multipolar switching, gives rise to more than one candidate pulse pattern that is considered in the conventional OPP problem. Specifically, it can be shown that there are  $2^{d+1} - 1$  candidate HWS OPPs. This implies that the HWS OPP optimization problem besides being non-convex (such as problem (2)), is also a mixed integer problem.

With the aforementioned changes, the revised optimization problem that accounts for the CMV constraint becomes

$$\begin{aligned}
 & \underset{\alpha_H, \mathbf{u}_H}{\text{minimize}} && J(\alpha_H, \mathbf{u}_H) = \sum_{n=5,7,11,\dots} \frac{a_n^2 + b_n^2}{n^2} \\
 & \text{subject to} && a_1 = 0, \quad b_1 = m \\
 & && 0 \leq \alpha_1 \leq \alpha_2 \leq \dots \leq \alpha_{2d} \leq \pi \\
 & && u_i \in \{-1, 0, 1\} \text{ and} \\
 & && u_{i+1} - u_i \in \{-1, 1\} \quad \forall i \in \{0, \dots, 2d-1\} \\
 & && u_{2d} = -u_0 \\
 & && \max(|u_o(\theta)|) \leq 1/3,
 \end{aligned} \tag{5}$$

where the HWS CM switch position  $u_o$  is calculated according to the procedure provided in Algorithm 1. Note that in (5),  $\alpha_H = [\alpha_1 \alpha_2 \dots \alpha_{2d}]^T$  is the vector of the  $2d$  switching angles, and  $\mathbf{u}_H = [u_0 u_1 \dots u_{2d-1}]^T$  is the switching sequence under consideration. Moreover, as with problem (2), only odd non-triplen harmonics are considered since even harmonics are zero due to the HWS, while triplen harmonics do not affect the current. Nevertheless,  $a_1 = 0$  such that the phase of the fundamental component is zero.

Finally, to avoid solving the mixed integer optimization problem (5), a single non-convex optimization problem is instead solved for each candidate pulse pattern. Subsequently, in a post-processing step, the switching angles and corresponding switching sequence with the minimum cost are selected as the global solution.

## III. NUMERICAL RESULTS

This section shows the optimization results for (a) QaHWS OPPs without limitations on the CMV (see problem (2)), (b) QaHWS OPPs with reduced CMV, (see problem (2) augmented with constraint (4)), and (c) HWS OPPs with reduced CMV (see problem (5)). OPPs in the (b) category are hereafter referred to as QaHWS CMV OPPs, while those in category (c) as HWS CMV OPPs. All OPPs are computed by considering an MV drive system consisting of a three-level inverter and a squirrel cage induction machine. The machine has a rated voltage of 3.3 kV, 2.12 kA rated current, 50 Hz nominal frequency, 0.25 per unit (p.u.) total leakage reactance, while the dc-link voltage of the inverter is  $V_{dc} = 5.2$  kV.

### A. Effect on Current TDD

The maximum CM switch position of QaHWS OPPs with  $d = 5$  and 6 are shown in Figs. 4(a) and 5(a), respectively, see the (blue) solid line. As can be seen, when the CMV is not constrained, the maximum value of the CM position is  $\max(|u_0|) = 2/3$  over a wide range of modulation indices,

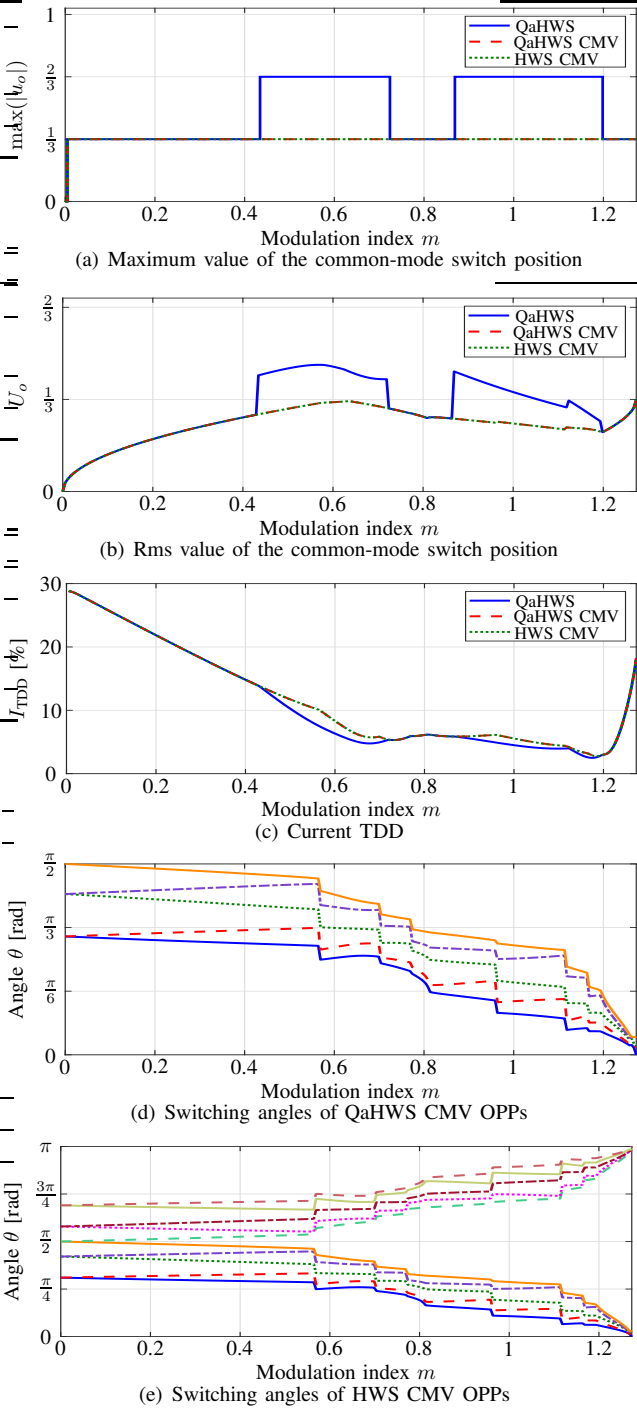


Fig. 4: QaHWS and HWS OPPs for  $d = 5$  without and with the CMV constraint. The solid (blue) line corresponds to the conventional QaHWS OPPs, the dashed (red) line to QaHWS CMV OPPs, and the dotted (green) line to HWS CMV OPPs.

namely  $m \in [0.434, 0.719] \cup [0.869, 1.193]$  for  $d = 5$  and  $m \in [0.344, 1.218]$  for  $d = 6$ . When the CMV constraint is implemented, the resulting QaHWS CMV OPPs reduce the CMV for all the aforementioned values of  $m$ . Additionally, the rms value of the CM switch position is also limited below  $1/3$ , as can be seen in Figs. 4(b) and 5(b) for the above-mentioned modulation index ranges. This, however, occurs at a cost of an increased current TDD, as can be observed in Figs. 4(c) and 5(c). Yet, for even pulse numbers, HWS CMV OPPs not only effectively reduce the CMV over the whole range of

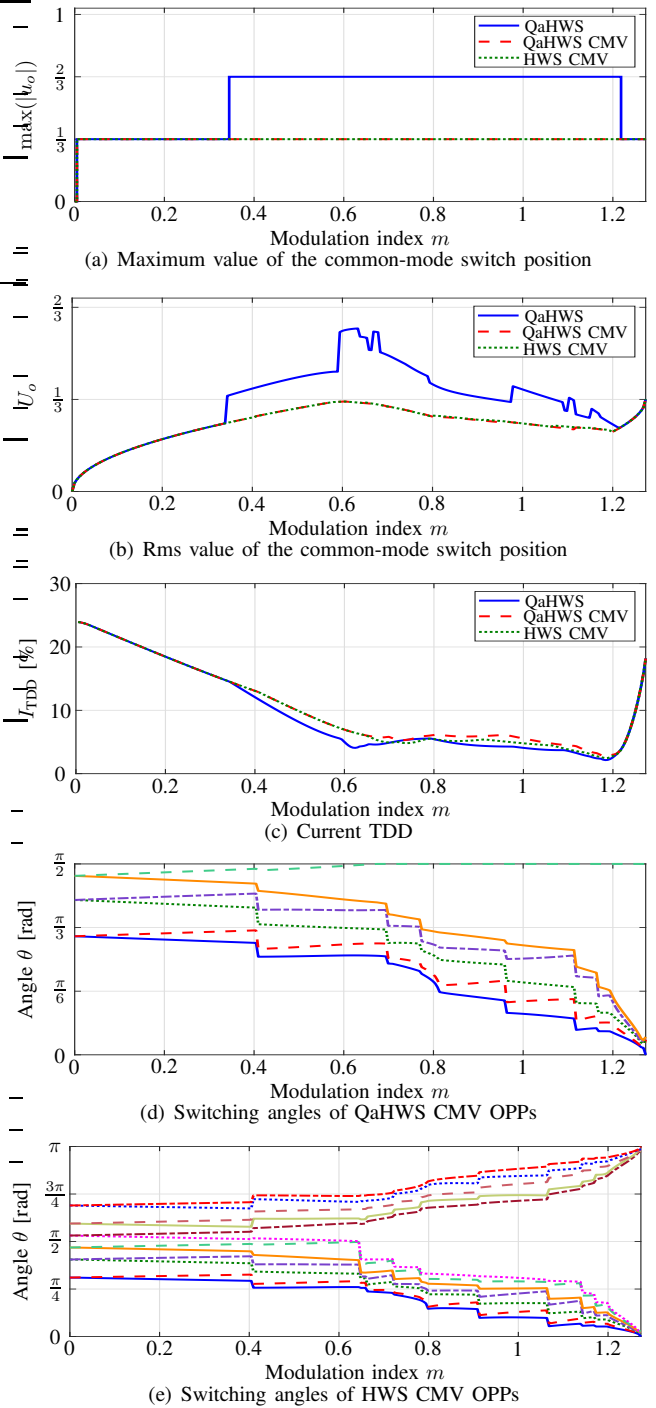


Fig. 5: QaHWS and HWS OPPs for  $d = 6$  without and with the CMV constraint. The solid (blue) line corresponds to the conventional QaHWS OPPs, the dashed (red) line to QaHWS CMV OPPs, and the dotted (green) line to HWS CMV OPPs.

modulation indices, but also do not significantly deteriorate the current TDD compared with conventional QaHWS OPPs.

To further investigate this, we define the *relative* current TDD as the normalized difference between the current TDD of CMV-constrained OPPs and conventional OPPs, i.e.,

$$I_{\text{TDD}}^{\text{rel}} = \frac{I_{\text{TDD,CMV}} - I_{\text{TDD,QaHWS}}}{I_{\text{TDD,QaHWS}}}. \quad (6)$$

As can be seen in Fig. 4(e), when odd pulse numbers are of interest, e.g.,  $d = 5$ , the OPPs computed with problem (5)

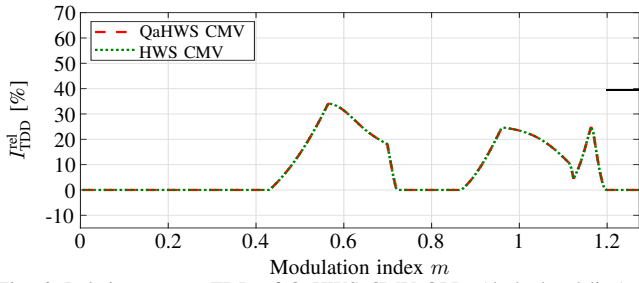


Fig. 6: Relative current TDD of QaHWS CMV OPPs (dashed red line) and HWS CMV OPPs (dotted green line) for  $d = 5$ .

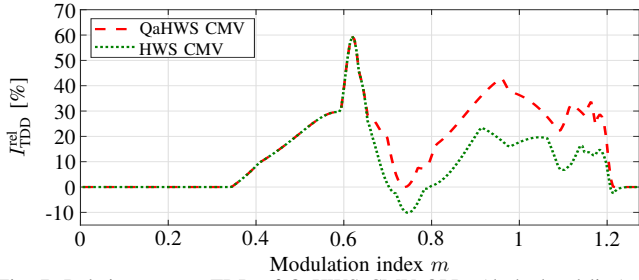


Fig. 7: Relative current TDD of QaHWS CMV OPPs (dashed red line) and HWS CMV OPPs (dotted green line) for  $d = 6$ .

do not exhibit HWS; QaHWS OPPs are returned over the whole range of modulation indices. As a result, the symmetry relaxations do not offer any advantages, leading to a maximum relative increase in  $I_{TDD}$  of 34.02% at  $m = 0.564$ , see Fig. 6. In general, the current TDD is compromised over a wide range of modulation indices, as anticipated.

In contrast to that, the symmetry relaxations offer significant advantages when even pulse numbers are considered, such as  $d = 6$ . As can be seen in Fig. 7, the maximum relative increase in  $I_{TDD}$  is 59.4% at  $m = 0.619$  when  $d = 6$ . This significant current TDD deterioration is because HWS CMV OPPs are not effective for modulation indices  $m < 0.68$  since QaHWS is observed in this range, see Fig. 5(e). However, at modulation indices where the HWS is active ( $m \geq 0.68$ ), the maximum relative increase in  $I_{TDD}$  is only 23.42% at  $m = 0.914$ . This is in contrast to the 43.02% increase in  $I_{TDD}$  of QaHWS CMV OPPs at  $m = 0.959$ , see Fig. 7. More impressively, compared with QaHWS OPPs, HWS CMV OPPs manage to reduce the current TDD for  $d = 6$  and modulation indices in the range  $[0.704, 0.794]$ . This is thanks to the additional degrees of freedom of problem (5), as it can distribute  $2d$  angles over a wider range of values. This point is highlighted in Fig. 5(e).

### B. Symmetry Relaxations

As can be seen in Fig. 4(e), the switching angles of the HWS CMV OPPs for  $d = 5$  (i.e., odd pulse numbers) exhibit QaHWS, with the symmetry relaxation providing no benefits. On the other hand, relaxing the quarter-wave symmetry leads to improved results for even pulse numbers. For  $m < 0.68$ , the OPPs with minimum  $I_{TDD}$  exhibit QaHWS, whereas OPPs exhibit QaHWS or HWS for  $m \geq 0.68$ . Moreover, QaHWS CMV OPPs drop one pulse in this range of modulation indices, see Fig. 5(d). This pulse-dropping feature of QaHWS CMV OPPs is due to the limitations imposed by properties (P1)–(P4). More specifically, for QaHWS OPPs, the pulse number determines if the phase- $a$  switch position of QaHWS OPPs is

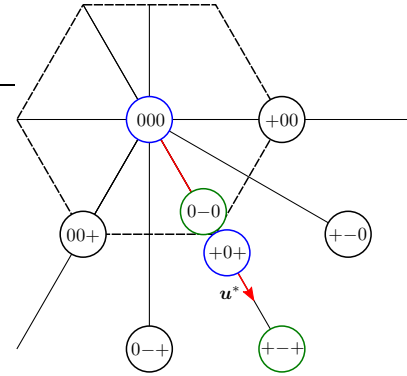


Fig. 8: Voltage vectors and corresponding three-phase switch positions of Example 1.

0 or 1 at  $\theta = \pi/2$ , i.e.,  $u_a(\frac{\pi}{2}) = 0$  or  $u_a(\frac{\pi}{2}) = 1$ , depending on whether  $d$  is even or odd, respectively. The results presented in this work suggest that for odd pulse numbers  $d$  (e.g.,  $d = 5$ ), the restriction of  $u_a(\frac{\pi}{2}) = 1$  respects the CMV constraint, and, therefore, lifting the quarter-wave symmetry property (P3) does not lead to improved results. On the other hand, it leads to a noteworthy improvement in the current TDD in the case of  $d = 6$ . This implies that the relaxation of the quarter-wave symmetry property (P3) is expected to lead to improved results when  $d$  is even. This is due to the restrictions that QaHWS poses to the CMV-constrained OPP problem when  $d$  is even. Specifically, as explained in the following example, these limitations lead to pulse dropping at high modulation indices.

**Example 1.** Consider QaHWS OPP with  $m > \frac{2}{3}$ . Assuming  $\theta = \frac{\pi}{6}$ , the fundamental component of the OPP  $\mathbf{u}^*$  in the  $\alpha\beta$ -plane is shown in Fig. 8. As can be seen,  $\mathbf{u}^*$  is aligned with the short vectors that correspond to the switch positions “0–0” and “+0+” as well as with the long vector with switch position “+–+”. Based on the observations presented in the appendix, the voltage sequence for the first  $\pi/6$  radians must end with a voltage vector on the symmetry axis. Given the symmetry property (P2),  $u_b(\vartheta) = -u(\vartheta + \frac{\pi}{3})$ , with  $\vartheta \in [0, \frac{\pi}{3}]$ , holds. This means that the phase- $b$  switch position is 0 or  $-1$  at  $\theta = \pi/6$ , i.e.,  $u_b(\frac{\pi}{6}) = 0$  or  $u_b(\frac{\pi}{6}) = -1$ , depending on whether  $d$  is even or odd, respectively, since  $u_a(\frac{\pi}{2}) = 0$  or  $u_b(\frac{\pi}{2}) = 1$ . In the former case, the possible voltage vectors that can be used to synthesize the desired modulation index require  $u_b(\frac{\pi}{6}) = 0$  and are shown as blue circles in Fig. 8. In the unconstrained problem, the voltage vector that corresponds to “+0+” is preferred, since it is the closest voltage vector to  $\mathbf{u}^*$  that satisfies the above requirements. However, this switch position cannot be used in the CMV-constrained problem since it has  $|u_o| = 2/3$ . In that case, the switch position to be applied at  $\theta = \frac{\pi}{6}$  will be the “000” one to satisfy the problem symmetries, see the appendix. However, when the modulation index is  $m > \frac{2}{3}$  then the modulating signal is outside the inner hexagon. As a result, using the switch position “000” leads to a major deviation between the output and desired voltage, giving rise to significant current distortions. If a pulse is dropped instead, the resulting OPP will have  $d - 1$  (i.e., an odd number of) pulses meaning that the possible voltage vectors that can be used to synthesize the desired modulation

index require  $u_b(\frac{\pi}{6}) = -1$  and are shown as green circles in Fig. 8. This way, the voltage vectors that correspond to switch positions “0–0” and “+–+” can be used to better approximate the desired modulation index.

For this reason, pulse dropping is preferred for QaHWS CMV OPPs to enable the use of a voltage vector that decreases the current distortions. HWS CMV OPPs, on the other hand, do not have to resort to pulse dropping as they can freely distribute the switching angles over  $\pi$  rads, and they can thus employ those voltage vectors that guarantee the lowest possible harmonics distortions.

Finally, it is worth mentioning that even though bipolar switching patterns are allowed in problem (5), the computed HWS CMV OPPs are exclusively unipolar patterns. As it turns out, bipolar switching leads to either infeasible or suboptimal patterns. This observation can be exploited to significantly reduce the computational complexity of problem (5), as it needs to be solved only for unipolar switching.

### C. Feasibility

As shown, when the CMV constraint is added the resulting QaHWS CMV OPPs reduce the CMV for all values of  $m$ . An important advantage of the proposed approach that limits the CMV (see Section II-D) is that OPPs with limited CMV can be computed for all pulse numbers  $d \geq 1$  over the whole range of modulation indices, i.e., the dc-link voltage is fully utilized even when the CMV is limited. If during the optimization process, the OPP with  $d$  pulses is suboptimal compared to that with  $d - 1$  pulses, unnecessary switching transitions (i.e., pulses) are avoided, and the (optimal) OPP with  $d - 1$  pulses is returned. Indeed, as mentioned before, QaHWS CMV OPPs with  $d = 6$  drop pulses for  $m \geq 0.68$ , see Fig. 5(d). In doing so, it is ensured that CMV-constrained OPPs are available for the whole range of modulation indices, and they produce as low harmonic distortions as possible.

## IV. COMPARISON WITH CB-PWM

This section compares the current harmonic performance of the computed OPPs with limited CMV with that of PWM techniques that can also limit the CMV. To this aim, phase-opposite disposition CB-PWM (PODPWM) is implemented along with the CB-PWM strategy proposed in [10], referred to as zero redundant state PWM (ZRSPWM). Both of these CB-PWM methods have a maximum CM switch position of  $1/3$  over the whole operating range. Additionally, optimal third-harmonic injection is considered for both PWM methods to extend the range of achievable modulation indices from  $[0, 1]$  to  $[0, 2/\sqrt{3}]$  without affecting the maximum CMV. For a direct and fair comparison in terms of produced current TDD, all examined PWM methods are designed to achieve synchronous modulation and generate pulse patterns with the same pulse number, namely  $d = 6$ .<sup>1</sup> As the SVM techniques that limit the CMV (see [11]–[13]) cannot achieve synchronous modulation

<sup>1</sup>To achieve this, the carrier-to-fundamental frequency ratio  $f_c/f_1$ , where  $f_c$  is the frequency of the carrier, is set to be an integer multiple of three [26], while the initial phase of the carriers is set such that QaHWS results [27].

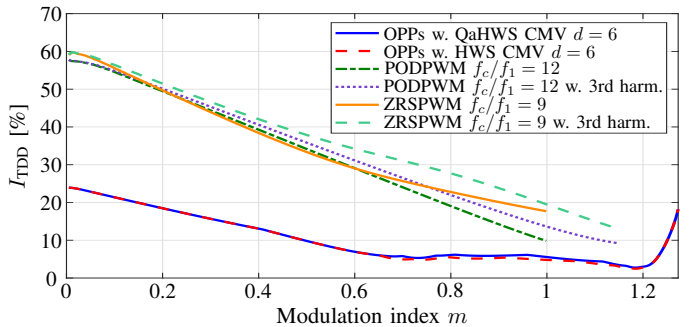


Fig. 9: Comparison of current TDD with different modulation techniques.

Parameter	Symbol	SI value
Rated line-to-line voltage	$V_R$	400 V
Rated stator current	$I_R$	5.8 A
Rated angular stator frequency	$\omega_R$	$2\pi 50$ rad/s
Dc-link voltage	$V_{dc}$	650 V
Total leakage inductance	$L_\sigma$	13 mH

TABLE I: System parameters for experimental setup

with six pulses, they are excluded from the comparisons presented in the sequel of the section.

For the framework described above, Fig. 9 shows the current TDD produced by each modulation method. From this figure, two main observations can be made. First, the CB-PWM methods result in comparable current TDD at lower modulation indices, while the performance of PODPWM improves as  $m$  increases. Moreover, the third harmonic injection deteriorates the current quality of both CB-PWM methods. Nevertheless, all CB-PWM methods produce currents of significantly lower quality than OPPs, regardless of the symmetry properties of the latter.

The second observation relates to the utilization of the dc-link voltage. As can be seen in Fig. 9, the examined CB-PWM methods underutilize the dc-link voltage as they can at most reach up to a modulation index of  $2/\sqrt{3}$  with a third-harmonic injection, while limiting the CM switch position to  $1/3$ . This is in contrast to OPPs, which, as also shown in Section III, can be used over the whole range of modulation indices. Therefore, OPPs that limit the CMV not only produce currents of much higher quality than the CB-PWM methods, but can also fully utilize the available dc-link voltage.

Based on the above, the presented results clearly demonstrate the potential of OPPs that can achieve both load-friendly operation—in terms of limited CMV and less thermal losses—and utilize the available hardware. Such features imply that considerable cost and energy savings can be achieved, making the proposed OPPs very relevant for MV drive systems.

## V. EXPERIMENTAL RESULTS

The numerical results presented in Section III for an MV drive system are experimentally verified hereafter with a scaled-down LV prototype. The real-world setup consists of a squirrel-cage induction machine and a three-level NPC SKiiP28MLI07E3V1 SEMIKRON converter. The system parameters are summarized in Table I. Note that the deadtime of the converter switches amounts to  $3.4 \mu\text{s}$ . To assess the

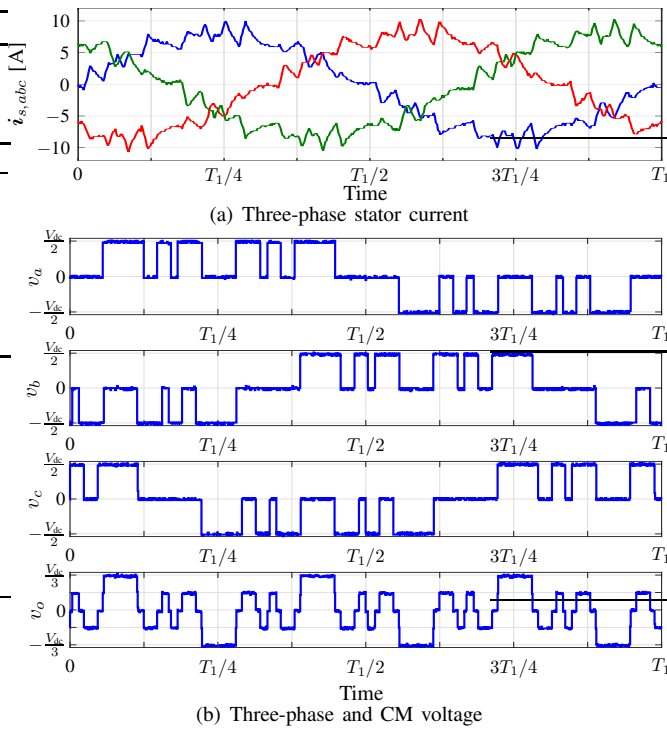


Fig. 10: Steady-state performance of an LV drive at  $m = 0.75$  when QaHWS OPPs with  $d = 6$  are used.

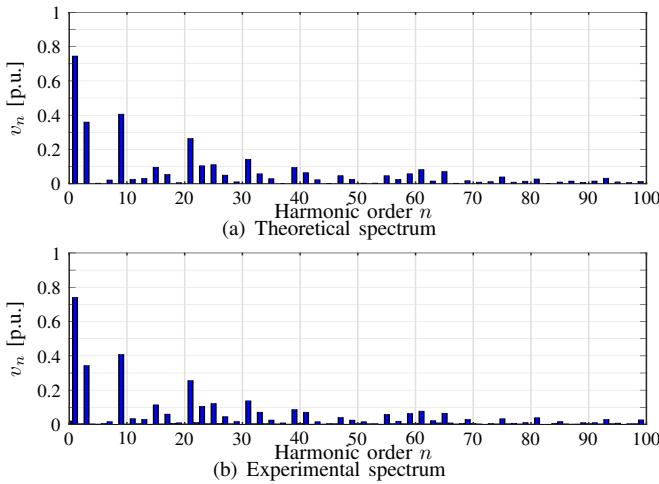


Fig. 11: Voltage spectrum at  $m = 0.75$  for QaHWS OPPs with  $d = 6$ .

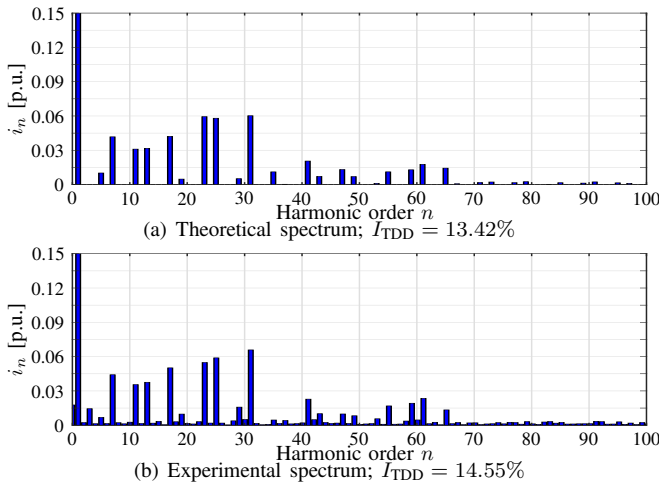


Fig. 12: Current spectrum at  $m = 0.75$  for QaHWS OPPs with  $d = 6$ .

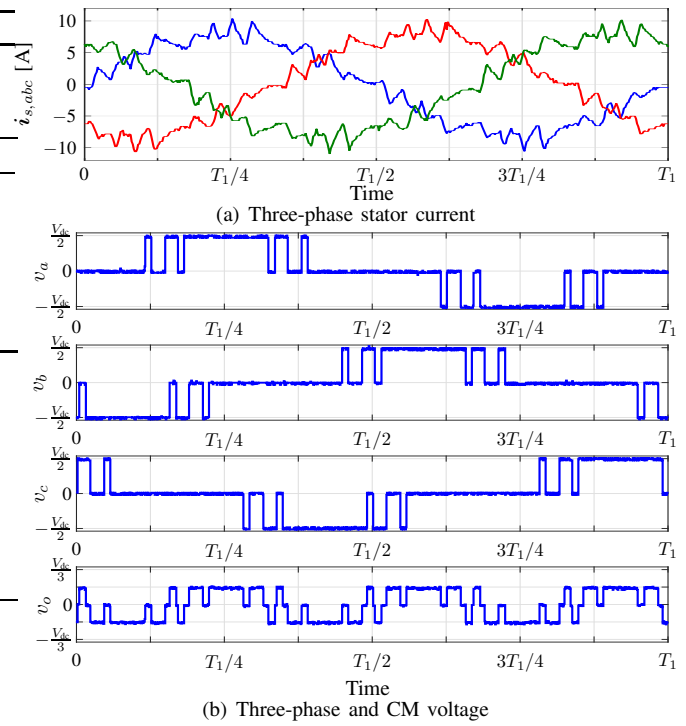


Fig. 13: Steady-state performance of an LV drive at  $m = 0.75$  when QaHWS CMV OPPs with  $d = 6$  are used.

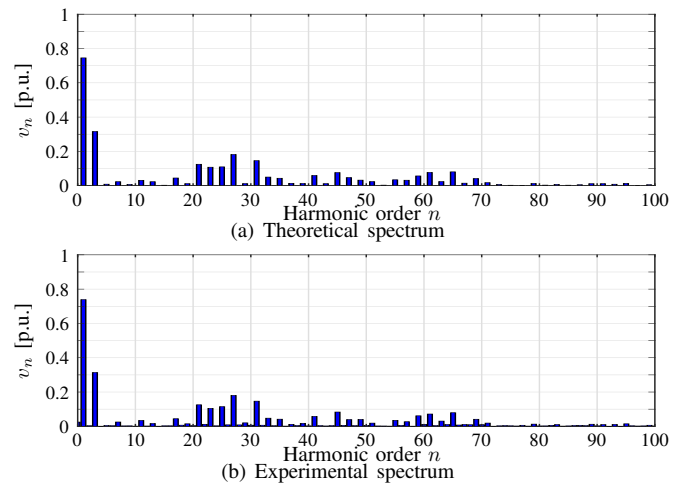


Fig. 14: Voltage spectrum at  $m = 0.75$  for QaHWS CMV OPPs with  $d = 6$ .

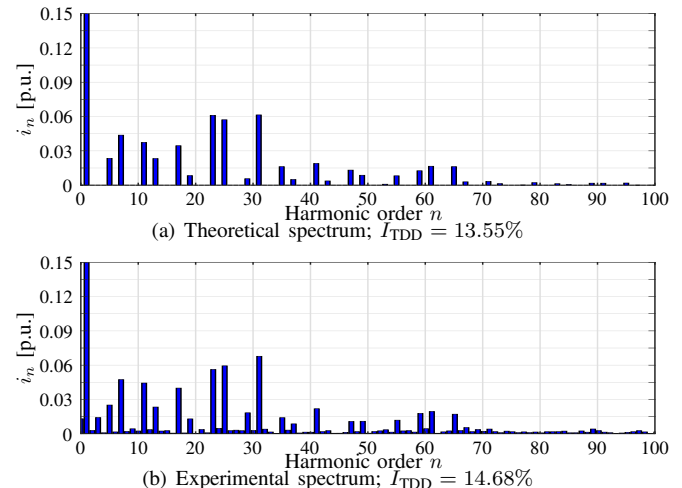


Fig. 15: Current spectrum at  $m = 0.75$  for QaHWS CMV OPPs with  $d = 6$ .

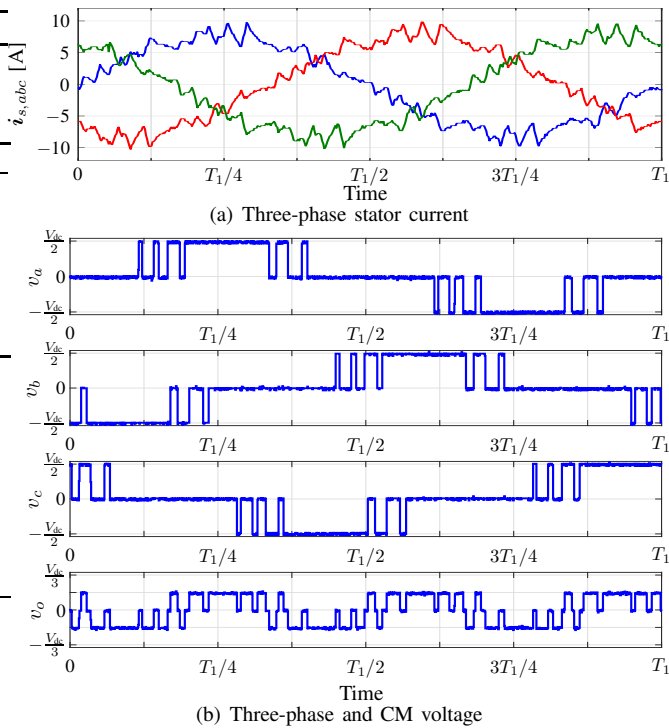


Fig. 16: Steady-state performance of an LV drive at  $m = 0.75$  when HWS CMV OPPs with  $d = 6$  are used.

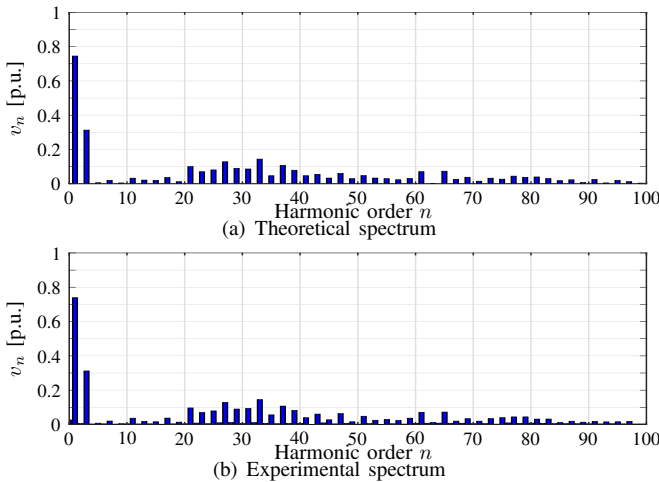


Fig. 17: Voltage spectrum at  $m = 0.75$  for HWS CMV OPPs with  $d = 6$ .

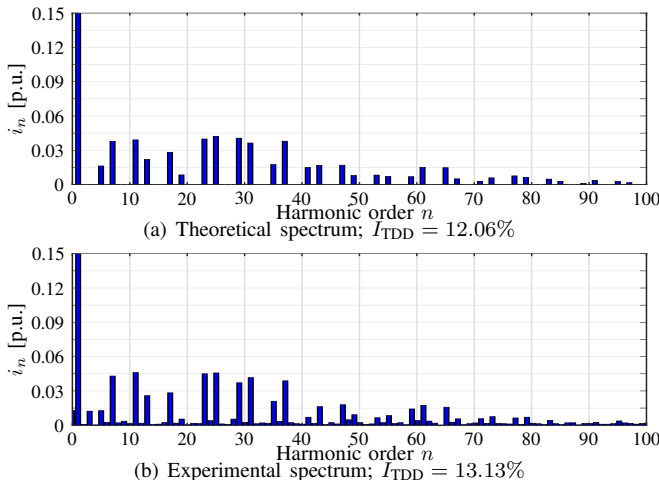


Fig. 18: Current spectrum at  $m = 0.75$  for HWS CMV OPPs with  $d = 6$ .

performance of the computed OPPs in a closed-loop setting, conventional scalar control is employed. To this aim, a dSPACE SCALEXIO system with a 2.8 GHz Intel i7-6820EQ processor and a Xilinx Kintex-7 field-programmable gate array (FPGA) serves as the control platform. The OPPs are stored as lookup tables (LUTs) in the processor of the dSPACE, and they are retrieved by the FPGA. Finally, the switch positions are generated in the FPGA and received by the inverter via digital inputs.

The examined OPPs have pulse number  $d = 6$ . For demonstration purposes, the steady-state performance of the LV drive is investigated at two different operating points, namely,  $m = 0.75$  and  $m = 1$ , while rated torque is considered. Figs. 10 to 18 relate to the first operating point, while Figs. 19 to 27 to the second. For each operating point, three different types of OPPs are assessed, i.e., QaHWS, QaHWS CMV, and HWS CMV OPPs.

Starting with the operating point that corresponds to modulation index  $m = 0.75$ , the performance of conventional QaHWS OPPs is examined first. As can be seen in Fig. 10(b), the CMV reaches a maximum value of  $\max(|v_o|) = \frac{2}{3} \cdot \frac{V_{dc}}{2} = \frac{V_{dc}}{3}$ , verifying the results in Fig. 5(a). The harmonic spectrum of the experimentally measured phase voltage is very close to the theoretical one, see Fig. 11, validating the correct implementation of the OPPs. As for the stator current (Fig. 10(a)), the profiles of the theoretical and experimental harmonic spectra look similar, see Fig. 12. Regarding the former, it is computed based on the theoretical OPP and the total leakage inductance reported in Table I. This leads to a spectrum where only non-triplen odd harmonics appear. Nevertheless, as second-order effects—such as deadtimes, measurement noise, common-mode current paths, machine parameter variations—exist in the experimental environment, some differences emerge in the spectrum of the experimentally measured phase current. These manifest themselves as additional low-order harmonics, albeit of low amplitude.<sup>2</sup> Therefore, despite the anticipated nonidealities of the real-world setting, the differences between the two spectra remain small.

As for the proposed CMV OPPs, whether they have QaHWS or HWS, the instantaneous CMV is limited to  $\frac{1}{3} \cdot \frac{V_{dc}}{2} = \frac{V_{dc}}{6}$ , see Figs. 13(b) and 16(b), respectively. Interestingly, as the chosen operating point relates to the modulation index  $m = 0.75$ , i.e., above the corner value of 0.68 (see Section III-C), and the pulse number is even, QaHWS CMV OPPs resort to pulse dropping to keep the CMV limited without sacrificing the current quality much. This feature can be clearly seen in Fig. 13(b), where five (instead of six) pulses appear in each half of the fundamental period. This feature, however, does not appear in HWS CMV OPPs as the switching angles can be spread over  $\pi$  (instead of  $\pi/2$ ) rads, thus allowing for a more flexible distribution of the switching events. As a result, six pulses appear in the HWS CMV OPPs, see Fig. 16(b). This symmetry relaxation has also a positive impact on the current TDD. More specifically, the amplitude of the current

<sup>2</sup>It is noteworthy that the stator resistance of LV machines cannot be considered negligible. This also introduces small differences between the theoretical and actual amplitudes of the current harmonics.

harmonics produced by HWS CMV OPPs (Fig. 18) is not only lower than those of QaHWS CMV OPPs (Fig. 15), as also quantified by the current TDD values (13.13% compared with 14.68%), but they are also lower than those of the conventional QaHWS OPPs (Fig. 12). Thus, these results clearly demonstrate that the symmetry relaxations allow for the effective limitation of the CMV, while (occasionally) enabling the reduction of the current TDD. Therefore, it can be concluded that despite the small discrepancies between theoretical and experimental current harmonic spectra, the relative experimental performance of the different types of OPPs fully supports the theoretical analysis and numerical results presented in Sections II and III.

With regards to the second operating point, similar observations can be made. For instance, the conventional QaHWS OPPs do not produce the desired CMV as the maximum value is  $\frac{2}{3} \cdot \frac{V_{dc}}{2} = \frac{V_{dc}}{3}$ , see Fig. 19(b). Hence, as shown in Fig. 21, even though the current TDD is as low as 11.33%, load-friendly operation is not fully achieved as the adverse effects of CMV are not mitigated. On the other hand, the proposed CMV OPPs can address the CMV-related negative effects as they successfully limit the CMV even at high modulation indices such as the chosen one, see Figs. 22(b) and 25(b) for the QaHWS and HWS CMV OPPs, respectively. Thus, even though this occurs at the expense of somewhat higher current distortions compared to the conventional OPPs, since QaHWS and HWS CMV OPPs produce current TDD of 16.03% and 13.99%, respectively, see Figs. 24 and 27, the benefits of the proposed OPPs remain in place as they provide the best possible compromise between the lowest possible current distortions and a limited CMV. Finally, it is worth noting that the symmetry relaxation again benefits the CMV OPPs as HWS allows for lower current distortions than those of QaHWS, see Figs. 27 and 24, respectively.

## VI. CONCLUSIONS

This paper presented the implementation of a constraint to limit the CMV of both QaHWS and HWS OPPs. Both types of OPPs successfully kept the CMV below a desired value. Moreover, as shown, the proposed symmetry relaxations not only enabled the mitigation of the anticipated—due to the CMV limitation—increase in the harmonic distortions but also improved the current TDD over a limited range of modulation indices. Alas, these improvements apply only to OPPs with even pulse numbers. Nevertheless, regardless of the pulse number, when comparing with other PWM methods that also limit the CMV, the current TDD improvement that is achieved with the proposed CMV OPPs can be impressive. Moreover, and in contrast to existing PWM methods, the proposed OPPs are suitable for the whole range of operating points. Hence, not only load-friendly operation is achieved—as demonstrated by the lower current distortions and limited CMV—but also full utilization of the dc-link voltage, thus enabling energy and cost savings. Finally, the effectiveness of the computed OPPs was verified with an LV prototype. As shown, the second-order effects that can affect the proposed modulation technique have small impact on the current quality.

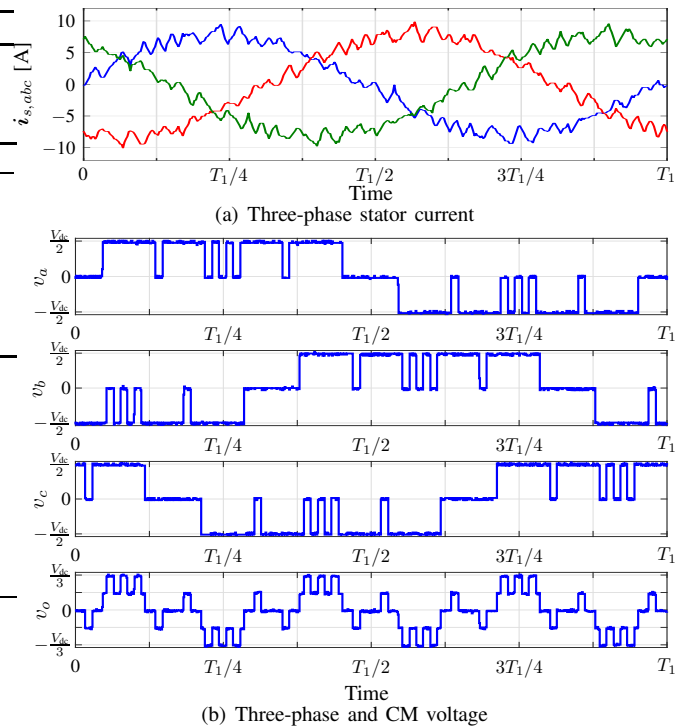


Fig. 19: Steady-state performance of an LV drive at  $m = 1$  when QaHWS OPPs with  $d = 6$  are used.

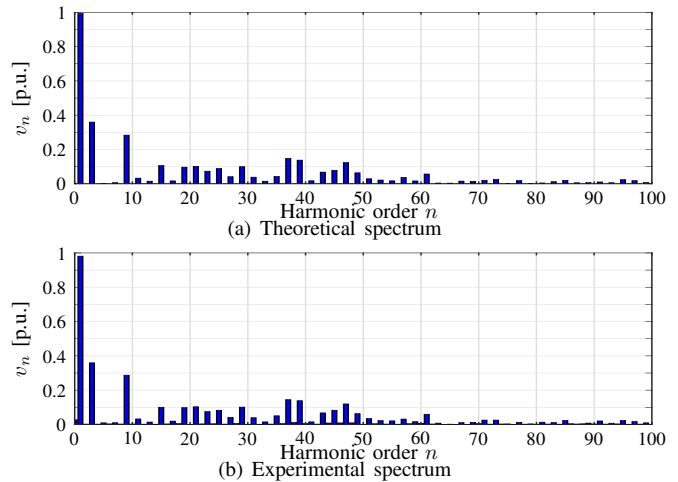


Fig. 20: Voltage spectrum at  $m = 1$  for QaHWS OPPs with  $d = 6$ .

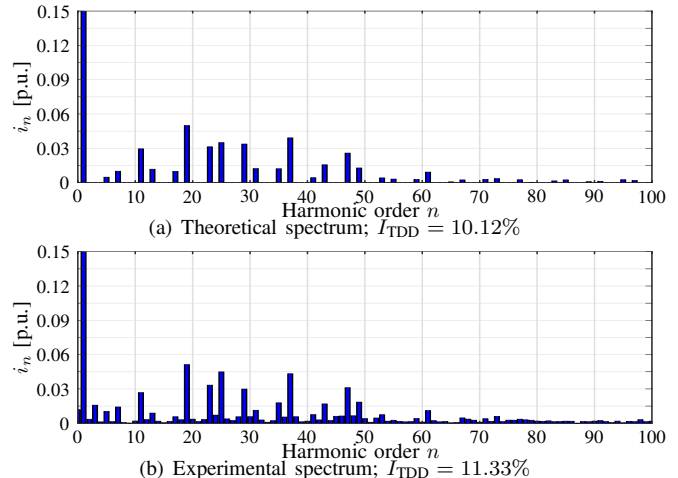


Fig. 21: Current spectrum at  $m = 1$  for QaHWS OPPs with  $d = 6$ .

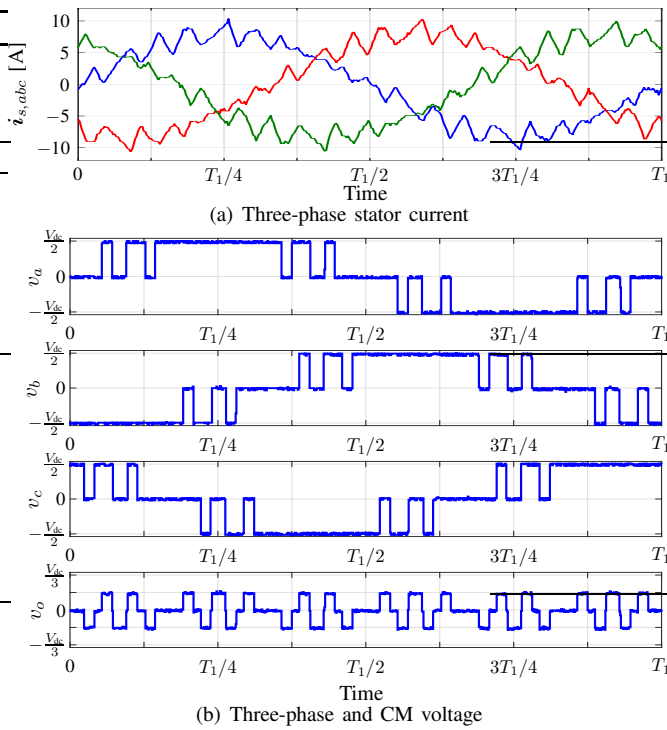


Fig. 22: Steady-state performance of an LV drive at  $m = 1$  when QaHWS CMV OPPs with  $d = 6$  are used.

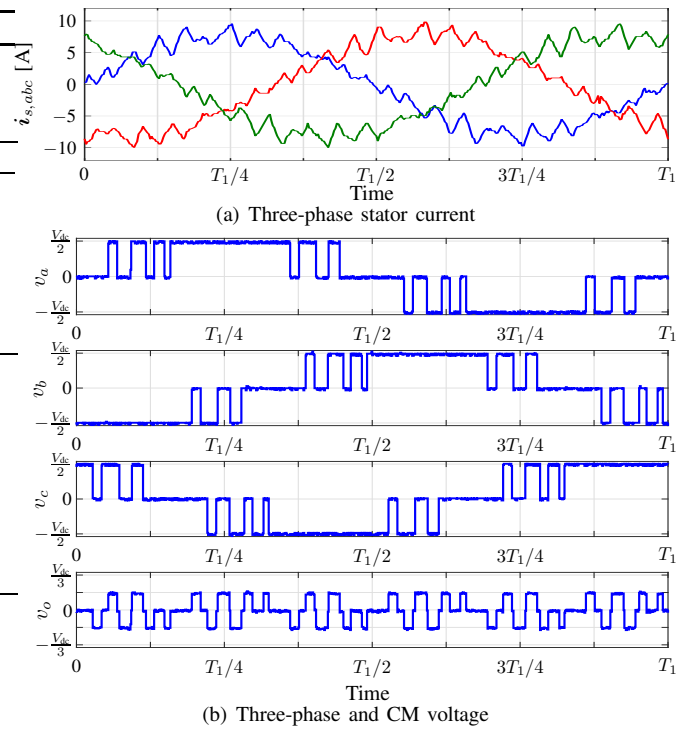


Fig. 25: Steady-state performance of an LV drive at  $m = 1$  when HWS CMV OPPs with  $d = 6$  are used.

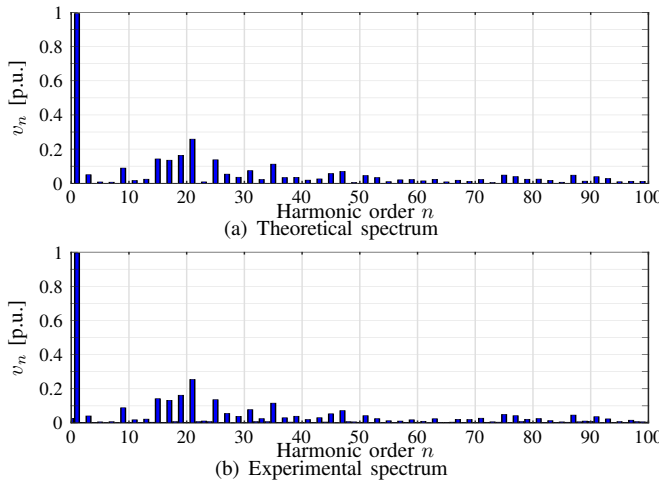


Fig. 23: Voltage spectrum at  $m = 1$  for QaHWS CMV OPPs with  $d = 6$ .

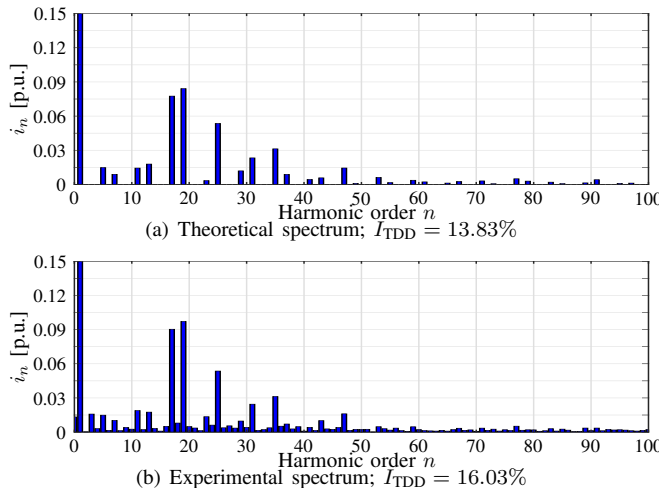


Fig. 24: Current spectrum at  $m = 1$  for QaHWS CMV OPPs with  $d = 6$ .

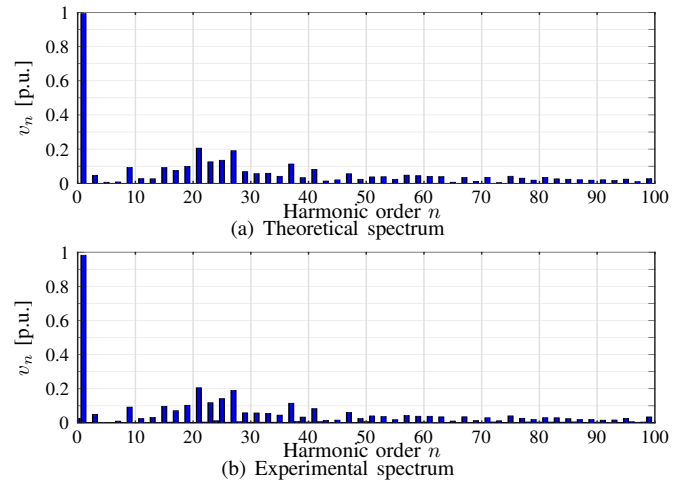


Fig. 26: Voltage spectrum at  $m = 1$  for HWS CMV OPPs with  $d = 6$ .

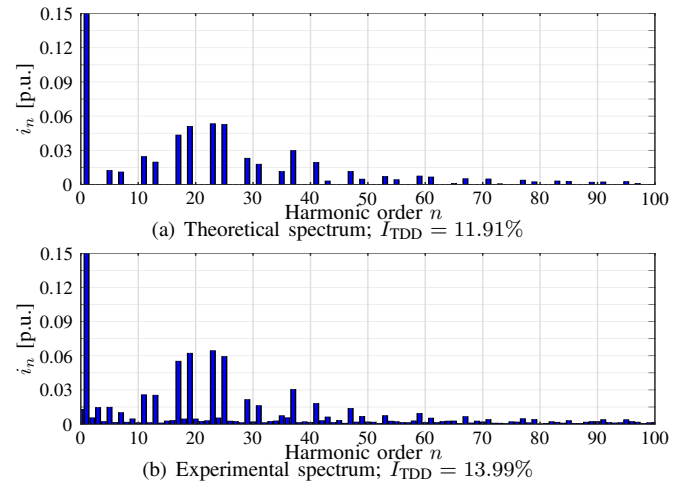


Fig. 27: Current spectrum at  $m = 1$  for HWS CMV OPPs with  $d = 6$ .

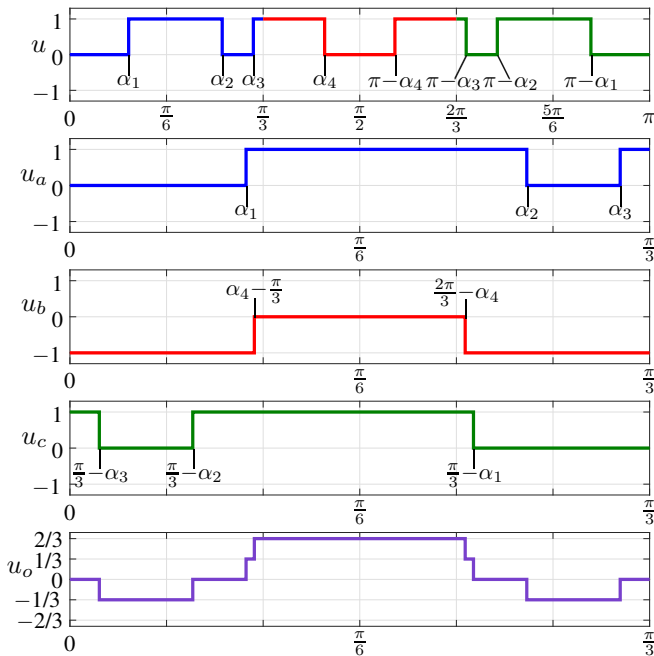


Fig. 28: Illustration of the calculation of the CM position  $u_o$  corresponding to the QaHWS OPP for  $d = 4$  at modulation index  $m = 0.8$

#### APPENDIX

The CM switch position  $u_o$ , and thus the CMV  $v_o$ , inherit the symmetry properties of a three-phase OPP presented in Section II-B. Specifically, if the OPP exhibits QaHWS then  $u_o$  will also exhibit QaHWS. It should be noted that these properties are also reflected in the sequence of voltage vectors in the  $\alpha\beta$ -plane. For demonstration purposes, consider the QaHWS OPP for  $d = 4$  and  $m = 0.8$ . The single-phase QaHWS OPP  $u$  is shown in the top subfigure of Fig. 28, while the CM switch position  $u_o$  over  $\pi/3$  radians, i.e., a half of its fundamental period, is depicted in the bottom subfigure.<sup>3</sup> Finally, the three-phase OPP  $u_{abc}$  over a sixth of its fundamental period is shown in between the above-mentioned subfigures.

As can be seen, the sequence of switch positions of the three-phase OPP  $u_{abc}$  within the first  $\pi/6$  radians is “0-+” at  $\pi/3-\alpha_3$  → “0-0” at  $\pi/3-\alpha_2$  → “0-+” at  $\alpha_1$  → “+-+” at  $\alpha_4-\pi/3$  → “+0+”. The sequence of the corresponding voltage vectors is shown in Fig. 29 with blue colors. The sequence of switch positions of the three-phase OPP  $u_{abc}$  within the second  $\pi/6$  radians is “+0+” at  $2\pi/3-\alpha_4$  → “+-+” at  $\pi/3-\alpha_1$  → “+-0” at  $\alpha_2$  → “0-0” at  $\alpha_3$  → “+-0”, see also Fig. 29 where the sequence of corresponding voltage vectors is shown with green colors. We observe that these two sequences are symmetric as they are mirrored with respect to the axis aligned with the short vectors that correspond to the switch positions “0-0” and “+0+” as well as the long vector resulting from the switch position “+-+”. This means that the sequence of voltage vectors in the first quarter of the fundamental period of the CM switch position must end in one of the voltage vectors on the said symmetry axis.

<sup>3</sup>Note that due to the QaHWS of the OPP, the full information of  $u_o$  is included in  $\pi/6$  radians. For illustration purposes, however, the CM switch position is depicted for half of its fundamental period.

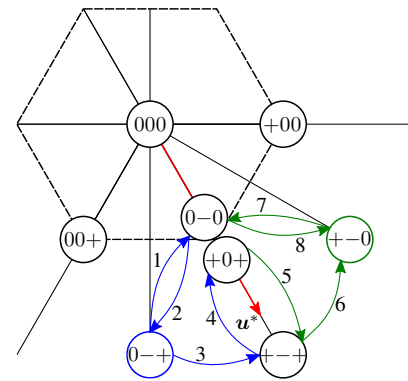


Fig. 29: Sequence of voltage vectors of the three-phase OPP in Fig. 28 over a sixth of the fundamental period. Note that  $u^*$  denotes the fundamental component of the OPP in the  $\alpha\beta$ -plane.

#### REFERENCES

- [1] L. G. Franquelo, J. Rodríguez, J. I. Leon, S. Kouro, R. Portillo, and M. A. M. Prats, “The age of multilevel converters arrives,” *IEEE Ind. Electron. Mag.*, vol. 2, no. 2, pp. 28–39, Jun. 2008.
- [2] A. Mütze and A. Binder, “Don’t lose your bearings—Mitigation techniques for bearing currents in inverter-supplied drive systems,” *IEEE Ind. Appl. Mag.*, vol. 12, no. 4, pp. 22–31, Jul./Aug. 2006.
- [3] F. T. Kheng Suan, N. A. Rahim, and H. W. Ping, “Three-phase transformerless grid-connected photovoltaic inverter to reduce leakage currents,” in *Proc. IEEE Conf. Clean Energy and Technol.*, Langkawi, Malaysia, Nov. 2013, pp. 277–280.
- [4] W.-J. Cha, K.-T. Kim, Y.-W. Cho, S.-H. Lee, and B. Kwon, “Evaluation and analysis of transformerless photovoltaic inverter topology for efficiency improvement and reduction of leakage current,” *IET Power Electron.*, vol. 8, no. 2, pp. 255–267, Feb. 2015.
- [5] L. Kai, J. Zhao, W. Wu, M. Li, L. Ma, and G. Zhang, “Performance analysis of zero common-mode voltage pulse-width modulation techniques for three-level neutral point clamped inverters,” *IET Power Electron.*, vol. 9, no. 14, pp. 2654–2664, Nov. 2016.
- [6] X. Zhang, D. Boroyevich, R. Burgos, P. Mattavelli, and F. Wang, “Impact and compensation of dead time on common mode voltage elimination modulation for neutral-point-clamped three-phase inverters,” in *Proc. IEEE Energy Convers. Congr. Expo. Asia*, Melbourne, VIC, Australia, Jun. 2013, pp. 1016–1022.
- [7] M. M. Renge and H. M. Suryawanshi, “Five-level diode clamped inverter to eliminate common mode voltage and reduce  $dv/dt$  in medium voltage rating induction motor drives,” *IEEE Trans. Power Electron.*, vol. 23, no. 4, pp. 1598–1607, Jul. 2008.
- [8] H.-J. Kim, H.-D. Lee, and S.-K. Sul, “A new PWM strategy for common-mode voltage reduction in neutral-point-clamped inverter-fed ac motor drives,” *IEEE Trans. Ind. Appl.*, vol. 37, no. 6, pp. 1840–1845, Nov./Dec. 2001.
- [9] M. M. Renge and H. M. Suryawanshi, “Multilevel inverter to reduce common mode voltage in ac motor drives using SPWM technique,” *J. Power Electron.*, vol. 11, no. 1, pp. 21–27, Jan. 2011.
- [10] M.-J. Tsai, H.-C. Chen, M.-R. Tsai, Y.-B. Wang, and P.-T. Cheng, “Evaluation of carrier-based modulation techniques with common-mode voltage reduction for neutral point clamped converter,” *IEEE Trans. Power Electron.*, vol. 33, no. 4, pp. 3268–3275, Apr. 2018.
- [11] K. D. Pham and N. V. Nguyen, “A reduced common-mode-voltage pulsewidth modulation method with output harmonic distortion minimization for three-level neutral-point-clamped inverters,” *IEEE Trans. Power Electron.*, vol. 35, no. 7, pp. 6944–6962, Jul. 2020.
- [12] X. Zhang, X. Wu, C. Geng, X. Ping, S. Chen, and H. Zhang, “An improved simplified PWM for three-level neutral point clamped inverter based on two-level common-mode voltage reduction PWM,” *IEEE Trans. Power Electron.*, vol. 35, no. 10, pp. 11 143–11 154, Oct. 2020.
- [13] W. Jiang, P. Wang, M. Ma, J. Wang, J. Li, L. Li, and K. Chen, “A novel virtual space vector modulation with reduced common-mode voltage and eliminated neutral point voltage oscillation for neutral point clamped three-level inverter,” *IEEE Trans. Ind. Electron.*, vol. 67, no. 2, pp. 884–894, Feb. 2020.
- [14] C. Xia, G. Zhang, Y. Yan, X. Gu, T. Shi, and X. He, “Discontinuous space vector PWM strategy of neutral-point-clamped three-level inverters for output current ripple reduction,” *IEEE Trans. Power Electron.*, vol. 32, no. 7, pp. 5109–5121, Jul. 2017.

- [15] H. S. Patel and R. G. Hoft, "Generalized techniques of harmonic elimination and voltage control in thyristor inverters: Part I—Harmonic elimination," *IEEE Trans. Ind. Appl.*, vol. IA-9, no. 3, pp. 310–317, May/Jun. 1973.
- [16] G. S. Buja and G. B. Indri, "Optimal pulsewidth modulation for feeding ac motors," *IEEE Trans. Ind. Appl.*, vol. IA-13, no. 1, pp. 38–44, Jan./Feb. 1977.
- [17] Z. Zhao, Y. Zhong, H. Gao, L. Yuan, and T. Lu, "Hybrid selective harmonic elimination PWM for common-mode voltage reduction in three-level neutral-point-clamped inverters for variable speed induction drives," *IEEE Trans. Power Electron.*, vol. 27, no. 3, pp. 1152–1158, Mar. 2012.
- [18] M. Wu, C. Xue, Y. W. Li, and K. Yang, "A generalized selective harmonic elimination PWM formulation with common-mode voltage reduction ability for multilevel converters," *IEEE Trans. Power Electron.*, vol. 36, no. 9, pp. 10753–10765, Sep. 2021.
- [19] M. Sharifzadeh, M. Babaie, G. Chouinard, K. Al-Haddad, R. Portillo, L. G. Franquelo, and K. Gopakumar, "Hybrid SHM-PWM for common-mode voltage reduction in three-phase three-level NPC inverter," *IEEE J. Emerg. Sel. Topics Power Electron.*, vol. 9, no. 4, pp. 4826–4838, Aug. 2021.
- [20] J. M. D. Murphy and M. G. Egan, "A comparison of PWM strategies for inverter-fed induction motors," *IEEE Trans. Ind. Appl.*, vol. IA-19, no. 3, pp. 363–369, May/Jun. 1983.
- [21] I. Tsoumas, "On the computation of optimized pulse patterns with zero common mode voltage," in *Proc. Eur. Conf. on Power Electron. and Applicat.*, Genova, Italy, Sep. 2019, pp. P.1–P.10.
- [22] P. Hokayem, I. Pejic, and N. Oikonomou, "Optimal current trajectories for power converters with minimal common mode voltage," *IFAC World Congr.*, vol. 50, no. 1, pp. 2107–2112, Jul. 2017.
- [23] I. Koukoulou, P. Karamanakos, and T. Geyer, "Three-level optimized pulse patterns with reduced common-mode voltage," in *Proc. IEEE Energy Convers. Congr. Expo.*, Detroit, MI, USA, Oct. 2022, pp. 1–8.
- [24] A. Birth, T. Geyer, H. d. T. Mouton, and M. Dorfling, "Generalized three-level optimal pulse patterns with lower harmonic distortion," *IEEE Trans. Power Electron.*, vol. 35, no. 6, pp. 5741–5752, Jun. 2020.
- [25] A. K. Gupta and A. M. Khambadkone, "A space vector modulation scheme to reduce common mode voltage for cascaded multilevel inverters," *IEEE Trans. Power Electron.*, vol. 22, no. 5, pp. 1672–1681, Sep. 2007.
- [26] Z. Gao, Y. Li, Q. Ge, K. Wang, M. Zhao, and J. Zhu, "Research on the synchronized carrier-based PWM strategy under low switching frequency for three-level neutral point clamped inverter," in *Proc. IEEE Ind. Electron. Conf.*, Singapore, Oct. 2020, pp. 4121–4126.
- [27] J. Shen, S. Schröder, H. Stagge, and R. W. De Doncker, "Impact of modulation schemes on the power capability of high-power converters with low pulse ratios," *IEEE Trans. Power Electron.*, vol. 29, no. 11, pp. 5696–5705, Nov. 2014.

**Isavella Koukoulou** (S'22) received the Diploma degree in electrical and computer engineering from the National Technical University of Athens (NTUA), Athens, Greece, in 2021.

Since 2021, she has been with the Faculty of Information Technology and Communication Sciences, Tampere University, Tampere, Finland, where she is currently pursuing the Ph.D. degree in electrical engineering. Her main research interests lie at the intersection of optimal modulation, mathematical programming, and power electronics.



Miss Koukoulou received the Third Prize Paper Award of the Industrial Drives Committee at the 2022 IEEE Energy Conversion Congress and Exposition.



**Petros Karamanakos** (M'14 – SM'19) received the Diploma and Ph.D. degrees in electrical and computer engineering from the National Technical University of Athens (NTUA), Athens, Greece, in 2007, and 2013, respectively.

From 2010 to 2011 he was with the ABB Corporate Research Center, Baden-Dättwil, Switzerland, where he worked on model predictive control strategies for medium-voltage drives. From 2013 to 2016 he was a PostDoc Research Associate in the Chair of Electrical Drive Systems and Power Electronics, Technische Universität München, Munich, Germany. Since 2016, he has been with the Faculty of Information Technology and Communication Sciences, Tampere University, Tampere, Finland, where he is currently an Associate Professor. His main research interests lie at the intersection of optimal control, mathematical programming, and power electronics, including model predictive control and optimal modulation for utility-scale power converters and ac variable speed drives.

Dr. Karamanakos received the 2014 Third Best Paper Award of the IEEE Transactions on Industry Applications and four Prize Paper Awards at IEEE conferences. He serves as an Associate Editor of the IEEE Transactions on Industry Applications. He is a Regional Distinguished Lecturer of the IEEE Power Electronics Society in the years 2022 and 2023.



**Tobias Geyer** (M'08 – SM'10 – F'22) received the Dipl.-Ing. degree in electrical engineering, the Ph.D. in control engineering, and the Habilitation degree in power electronics from ETH Zurich, Zurich, Switzerland, in the years 2000, 2005, and 2017, respectively.

After his Ph.D., he spent three years at GE Global Research, Munich, Germany, three years at the University of Auckland, Auckland, New Zealand, and eight years at ABB's Corporate Research Centre, Baden-Dättwil, Switzerland. In 2020, he joined ABB's Medium-Voltage Drive division as R&D platform manager of the ACS6080. In 2022, he became a Corporate Executive Engineer. He has been an extraordinary Professor at Stellenbosch University, Stellenbosch, South Africa, since 2017.

He is the author of more than 40 patent families, 160 publications and the book "Model predictive control of high power converters and industrial drives" (Wiley, 2016). He teaches a regular course on model predictive control at ETH Zurich. His research interests include medium-voltage and low-voltage drives, utility-scale power converters, optimized pulse patterns and model predictive control.

Dr. Geyer received the IEEE PELS Modeling and Control Technical Achievement Award in 2022, the Semikron Innovation Award in 2021, and the Nagamori Award in 2021. He also received two Prize Paper Awards of IEEE Transactions and three Prize Paper Awards at IEEE conferences. He is a former Associate Editor of the IEEE Transactions on Industry Applications (from 2011 until 2014) and the IEEE Transactions on Power Electronics (from 2013 until 2019). He was an International Program Committee Vice Chair of the IFAC conference on Nonlinear Model Predictive Control in Madison, WI, USA, in 2018. Dr. Geyer was a Distinguished Lecturer of the IEEE Power Electronics Society from 2020 until 2023.

Dr. Geyer received the IEEE PELS Modeling and Control Technical Achievement Award in 2022, the Semikron Innovation Award in 2021, and the Nagamori Award in 2021. He also received two Prize Paper Awards of IEEE Transactions and three Prize Paper Awards at IEEE conferences. He is a former Associate Editor of the IEEE Transactions on Industry Applications (from 2011 until 2014) and the IEEE Transactions on Power Electronics (from 2013 until 2019). He was an International Program Committee Vice Chair of the IFAC conference on Nonlinear Model Predictive Control in Madison, WI, USA, in 2018. Dr. Geyer was a Distinguished Lecturer of the IEEE Power Electronics Society from 2020 until 2023.